

Article

Promotional Effect of Gold on the WGS Activity of Alumina-Supported Copper-Manganese Mixed Oxides

Tatyana Tabakova ^{1,*} , Ivan Ivanov ¹, Yordanka Karakirova ¹, Daniela Karashanova ², Anna Maria Venezia ³ , Petya Petrova ¹, Georgi Avdeev ⁴, Elitsa Kolentsova ⁵ and Krasimir Ivanov ⁵

¹ Institute of Catalysis, Bulgarian Academy of Sciences, 1113 Sofia, Bulgaria; bogoev@ic.bas.bg (I.I.); daniepr@ic.bas.bg (Y.K.); petia@ic.bas.bg (P.P.)

² Institute of Optical Materials and Technologies, Bulgarian Academy of Sciences, 1113 Sofia, Bulgaria; dkarashanova@gmail.com

³ Istituto per lo Studio dei Materiali Nanostrutturati, CNR, 90146 Palermo, Italy; annamaria.venezia@ismn.cnr.it

⁴ Institute of Physical Chemistry, Bulgarian Academy of Sciences, 1113 Sofia, Bulgaria; g_avdeev@ipc.bas.bg

⁵ Department of Chemistry, Agricultural University, 4000 Plovdiv, Bulgaria; elitsa_kolentsova@abv.bg (E.K.); kivanov1@abv.bg (K.I.)

* Correspondence: tabakova@ic.bas.bg; Tel.: +359-297-925-28

Received: 29 September 2018; Accepted: 26 October 2018; Published: 20 November 2018



Abstract: The water-gas shift (WGS) reaction is a well-known industrial process used for the production of hydrogen. During the last few decades, it has attracted renewed attention due to the need for high-purity hydrogen for fuel-cell processing systems. The aim of the present study was to develop a cost-effective and catalytically efficient formulation that combined the advantageous properties of transition metal oxides and gold nanoparticles. Alumina-supported copper-manganese mixed oxides were prepared by wet impregnation. The deposition-precipitation method was used for the synthesis of gold catalysts. The effect of the Cu:Mn molar ratio and the role of Au addition on the WGS reaction's performance was evaluated. Considerable emphasis was put on the characterization of the as-prepared and WGS-tested samples by means of a number of physicochemical methods (X-ray powder diffraction, high-resolution transmission electron microscopy, electron paramagnetic resonance, X-ray photoelectron spectroscopy, and temperature-programmed reduction) in order to explain the relationship between the structure and the reductive and WGS behavior. Catalytic tests revealed the promotional effect of gold addition. The best performance of the gold-promoted sample with a higher Cu content, i.e., a Cu:Mn molar ratio of 2:1 might be related to the beneficial role of Au on the spinel decomposition and the highly dispersed copper particle formation during the reaction, thus, ensuring the presence of two highly dispersed active metallic phases. High-surface-area alumina that was modified with a surface fraction of Cu-Mn mixed oxides favored the stabilization of finely dispersed gold particles. These new catalytic systems are very promising for practical applications due to their economic viability because the composition mainly includes alumina (80%).

Keywords: gold catalysts; WGS; copper-manganese mixed oxides; hydrogen production

1. Introduction

The development of energy devices with a high efficiency and environmental friendliness contributes to the future of sustainable energy, thus, improving the quality of life. The advancements in fuel-cell processing technology stimulated intensive research of the water-gas shift (WGS) reaction

because of its importance in hydrogen production [1]. This reaction is well known due to its long application as an industrially important process for the CO removal in the syngas, coupled with additional hydrogen generation. In order to avoid the kinetic and thermodynamic constraints, two reactors in series, involving high temperature and low-temperature WGS processes, are employed industrially [2]. Copper is widely used as an active component in commercially applicable WGS catalysts for large-scale hydrogen production due to its activity at low temperatures and its lower cost in comparison to the noble metals. Recently, the evaluation of the WGS catalytic behavior of mixed copper-manganese oxides pointed out the promising opportunity for their practical application [3–9]. The effect of different preparation methods and experimental conditions was studied in order to improve catalyst activity and stability. Zhi et al. have investigated the effect of the basifying agent (KOH or NaOH) used during the co-precipitation of the textural and structural properties of copper-manganese mixed oxides [5]. The rate of the precipitator addition into the reactor, as well as the type of copper-manganese salt precursors (nitrates, sulfates, acetates, and chlorides), has influenced the texture and WGS activity significantly [6,7]. Special attention was paid to the role of the catalyst composition. The impact of the Cu:Mn ratio on the structure, the WGS activity, and on the stability of the Cu-Mn mixed oxides was investigated [8]. The authors ascribed a higher activity of the sample with a Cu to Mn ratio of 1:1 to its higher surface area and the synergistic interaction between copper and manganese.

The addition of a third component was also studied as a relevant approach for improving the catalytic performance of Cu-Mn mixed oxides. Doped Cu–Mn–M spinel catalysts (M = Ce, Zr, Zn, Fe, Al) were synthesized by a single step combustion method and a different effect was observed depending on the nature of dopants [10]. The addition of Zr and Fe significantly enhanced the WGS activities, while the promotion by Ce, Zn, or Al had a detrimental effect. He et al. modified the Cu-Mn catalytic system with 0.5–10.0 mol % La and examined its impact on the structural and catalytic properties at low temperatures [11]. An improvement in the reducibility and more homogeneous distribution of Cu and Mn that correlate well with the WGS performance were attained after doping with a rather low amount of lanthanum. Cu-Mn-Ce metal oxide catalysts were prepared by the nano-casting method and a higher WGS activity was demonstrated in comparison to binary metal oxide samples [12].

However, the Cu-based catalysts are not always suitable for mobile applications because they are pyrophoric, intolerant to poisons, are susceptible to oxidation and condensation, and require a careful activation procedure before use. These drawbacks could be overcome by using noble metal-based catalysts. Among them, gold-based catalysts have attracted an exceptional interest due to their promising WGS behavior in the low-temperature range [13–19]. In 1995, Andreeva et al. reported a high WGS activity of finely dispersed gold on α -Fe₂O₃ [13]. The superior WGS performance of gold-based catalysts in comparison to commercial CuO/ZnO/Al₂O₃ was observed for the first time. In the same study, an Au/Al₂O₃ sample with a gold particles size that was similar to those in Au/ α -Fe₂O₃ exhibited very low activity, thus, focusing on a crucial role of support nature. Afterward, the effect of various metal oxides (Fe₂O₃, TiO₂, CeO₂, ZrO₂, Co₃O₄, etc.), including materials with different structures and morphologies—such as mixed or doped metal oxides—on the WGS activity of gold catalysts was examined [17,18]. Numerous papers focused on Au/ceria or doped ceria and addressed the impact of different factors, including the preparation method, the amount of gold, and support surface area, the nature and reactivity of the active gold species, the gold particle size, the structure, and the oxidation state on the catalytic performance in the WGS [19].

Recently, a new strategy for the optimization of the WGS performance of gold-based catalysts was proposed by the Odriozola group. In an attempt to develop active and cost-effective catalytic materials, efforts were directed into the reduction of the content of rare earth oxides in the catalyst composition by using alumina promoted with M-doped ceria (M = Fe, Zn, Co, Cu) as a support [20–22]. The dispersion of the metal oxide phase on high-surface-area alumina provided the possibility to enhance the reducibility and to improve the oxygen mobility of the gold catalysts. Very recently,

the same group reported that the gold nanoparticles deposited on a commercial-like Cu-Zn-Al support prepared from a hydrotalcite precursor could be a very efficient WGS catalyst [23]. The equilibrium CO conversion was achieved at 180 °C. In addition to the excellent activity, a high stability during the long-term and start-up/shut-down experiments was observed.

Considering the advantageous features in the WGS of both gold-based catalysts and Cu-Mn mixed oxides as a starting point, we aimed to design a catalytically active and economically feasible formulation by means of the deposition of gold nanoparticles on alumina supported by Cu-Mn mixed oxides. Various techniques (Nitrogen sorption, Powder X-ray diffraction, High-resolution transmission electron microscopy, Electron paramagnetic resonance, X-ray photoelectron spectroscopy, and temperature programmed reduction) were used to characterize the structural, electronic, and redox properties of the fresh and tested samples and to clarify the effect of the Cu:Mn molar ratio and the promotional role of gold on the WGS activity.

2. Results and Discussion

2.1. Catalytic Activity Measurements

The effect of the Cu:Mn molar ratio on the WGS activity is illustrated in Figure 1a where the temperature dependence of CO conversion over γ -Al₂O₃-supported Cu-Mn mixed oxides with a Cu-to-Mn ratio of 2:1 and 1:5 were compared. These two compositions were selected based on a recent study of the impact of the Cu:Mn ratio on CO oxidation activity [24]. Catalytic measurements indicated that the addition of MnO₂ to CuO/Al₂O₃ caused a significant increase in activity. This effect was valid for the whole concentration range of mixed oxides and a sharp decrease of the CO oxidation conversion was observed with MnO₂/Al₂O₃. In the present work, the WGS activity of alumina-supported CuO and MnO₂ were also studied for comparison. Experiments were carried out up to 260 °C within the low-temperature WGS reaction interval of interest. CO conversion data were collected by a heating step of 20 °C after attaining a stationary conversion at each step. In this way, reliable information was provided if the CO conversion resulted only from the WGS reaction and no CO consumption as for example for CO oxidation or CuO reduction occurred. Above 180 °C, catalytic activity results clearly showed a synergistic effect of the interaction between copper oxide and manganese oxides. Both alumina-supported Cu-Mn mixed oxides exhibited a similar activity that was higher relative to that of the supported mono metal oxides. Between the latter two samples, a better CO conversion was measured over CuO/Al₂O₃ in agreement with the well-known high low-temperature WGS activity of copper-based materials. Sample labeling in accordance with sample composition is described in the Experimental section.

The promotional role of gold on WGS performance was evaluated with alumina-supported mixed oxides. The temperature dependence of CO conversion is demonstrated in Figure 1b. Both gold-containing catalysts were more active than the corresponding Cu-Mn mixed oxides supported on the alumina. The highest catalytic activity was exhibited by gold on a Cu-rich sample, i.e., with a Cu-to-Mn ratio of 2:1. The added gold significantly enhanced its activity, namely, a higher CO conversion (40%) was attained at 200 °C as compared to other samples. Additionally, the CO conversion almost reached the equilibrium value (96.5%) at 260 °C. On the contrary, the modification of the Mn-rich material with gold caused only a slight improvement of activity. The favorable role of the Cu-Mn mixed oxide phase on the WGS activity of the gold-promoted catalyst was evidenced by comparison with the behavior of alumina-supported gold catalyst that exhibited a very low activity.

The discussion of beneficial catalytic performance should also include the evaluation of catalyst stability. It was assumed that small copper clusters are the active sites for the low-temperature WGS reaction over copper-based catalysts [2]. The presence of very small copper particles contributed to the highest CO conversion, while their sintering into larger agglomerates negatively affected the catalyst behavior [25]. The same statement is valid for the gold-based catalysts. A long-term stability test was performed at 260 °C with the most active Au/CuMn (2:1) sample. The experiment was

conducted within 4 days by starting every day with an increase of the temperature up to 260 °C, keeping it constant at 260 °C for 8 h, and then cooling down to room temperature. Figure S1 displays a plot of CO conversion as a function of time on stream. The results showed that the sample fully retained its catalytic activity after 32 h of work. An additional advantage of this formulation is that the measurements were performed without a preliminary reduction treatment, which represents the usual activation procedure for commercial copper-based WGS catalysts.

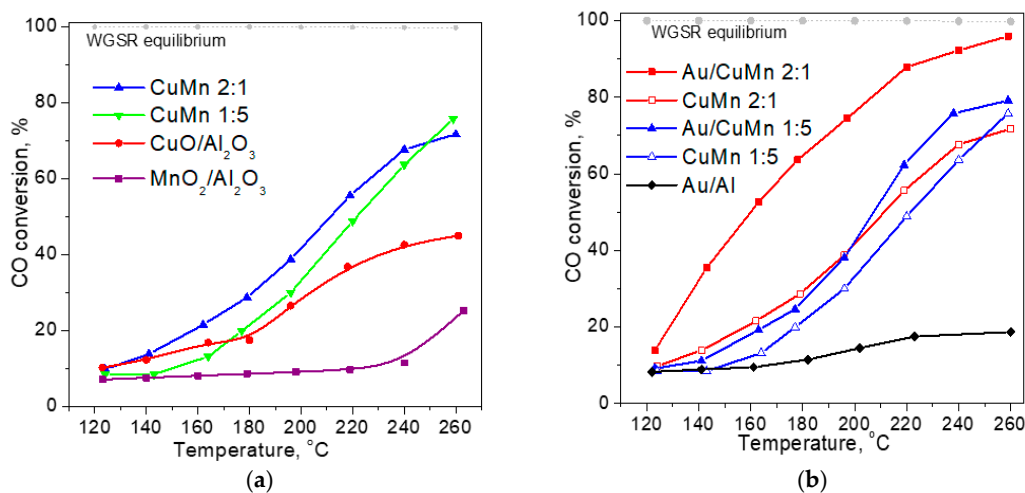


Figure 1. The temperature dependence of CO conversion during water-gas shift (WGS) reaction over (a) alumina-supported CuO, MnO₂, and mixed oxides with a Cu-to-Mn molar ratio of 2:1 and 1:5; (b) alumina-supported Cu-Mn mixed oxides with a Cu-to-Mn molar ratio of 2:1 and 1:5, and the respective gold-promoted samples.

It was mentioned in the Introduction section that one of the main drawbacks of the commercial copper-based catalysts is the reoxidation of the metallic copper species, which occurs during exposure of the used catalysts to the air. This process leads to the sintering of the copper nanoparticles and could be the reason for irreversible deactivation. Further catalytic measurements were performed with all the samples in order to prove the effect of reoxidation. After a catalytic test up to 260 °C, the reactor was cooled down to room temperature and the samples were kept in a CO/Ar mixture for about 15 h. Then the samples were subjected to an oxidative treatment in air for 1 h and the WGS tests were repeated. All samples demonstrated the same CO conversion value, thus suggesting that reoxidation did not affect active copper sites.

2.2. Sample Characterization

2.2.1. Textural Properties

Table 1 shows specific surface area, pore volume, and average pore diameter of the metal oxide supports and related gold catalysts. A decrease in the specific surface area was observed after the impregnation of alumina. This finding together with a decreased pore volume indicated the penetration of mixed solution of copper and manganese nitrates into the pores and the subsequent deposition of metal oxide phases during thermal treatment. The deposited Au caused a slight decrease of surface area, with pore volume and pore diameter remaining almost unchanged.

Table 1. The specific surface area (S_{BET}), total pore volume (V_{total}), and average pore diameter (D_{av}) as estimated by physisorption measurements.

Sample	S_{BET} (m^2/g)	V_{total} (cm^3/g)	D_{av} (nm)
Al_2O_3	219	0.40	7.4
CuMn 2:1	177	0.31	7.1
CuMn 1:5	181	0.32	7.2
Au/CuMn 2:1	143	0.29	7.4
Au/CuMn 1:5	150	0.31	6.7

2.2.2. Thermal Analysis (DTA, DTG, and TG)

Results of differential thermal analysis (DTA), differential thermal gravimetry (DTG), and thermal gravimetry (TG) analysis of alumina-supported Cu-Mn mixed oxides with a Cu:Mn ratio of 2:1 and 1:5 are presented in Figure S2a,b and Table 2. Both samples showed four weight losses due to different decomposition steps. The first weight loss registered below 150 °C was related to the loss of hydration water and partial nitrate decomposition. The next two losses occurred at 150–300 °C and were attributed to nitrate decomposition. The last weight loss at 303 and 331 °C was associated with a highly dispersed mixture of CuO (CuMn 2:1) or MnO_2 (CuMn 1:5) and the formation of a Cu-Mn spinel, respectively. This analysis agrees with the experimental findings of Kondrat et al. [26] about the predominant presence of metal oxides in the active phase during decomposition of mixed copper and manganese acetate above 300 °C. Other evidence for stable spinel phase formation is the absence of well-expressed endothermic effect in the temperature range of 500–600 °C due to the decomposition of MnO_2 to Mn_2O_3 .

Table 2. The thermogravimetric data for alumina-supported Cu-Mn (2:1 and 1:5).

Sample	Weight Loss			
	First	Second	Third	Fourth
	Onset T, °C (Weight loss, %)			
CuMn 2:1	54 (5.3)	160 (12.9)	182 (5.9)	303 (6.4)
CuMn 1:5	46 (5.8)	148 (17.6)	190 (2.2)	331 (2.3)

2.2.3. X-Ray Powder Diffraction (XRD)

X-ray powder diffraction patterns of fresh (a) and WGS-tested (b) samples are given in Figure 2. Characteristic peaks of the γ -alumina support were detected in the diffractograms of all materials. Significant differences in the patterns of both alumina-supported Cu-Mn samples were observed (Figure 2a). The reflections at 2θ (35.6, 38.8, 48.6, and 61.8°) indicated the presence of CuO phase (marked with *) in the pattern of the fresh CuMn (2:1) sample. The shape of the peaks evidenced a high degree of crystallinity of the CuO particles. An average crystallite size of about 30 nm was calculated from the X-ray line broadening of the peaks at $2\theta = 35.6$ and 38.8°. Some reflections of MnO_2 (marked with o) were visible in the pattern of the CuMn (1:5) sample. Peak broadness could be related to poor crystallization of MnO_2 and to the presence of defects in the crystal structure. The average crystallite size was about 10 nm. This poor crystalline structure of the MnO_2 may contain structural defects, in particular, oxygen vacancies with an important role in enhancing the dissociative chemisorption of water. Pintons et al. have reported that manganese-based oxides of variable oxidation states promote the WGS reaction rate [27]. In addition to CuO and MnO_2 phases, the formation of a Cu-Mn spinel oxide phase could be suggested based on a thermal analysis.

Moreover, this expectation was consistent with the Cu-Mn-O phase diagram presented by Wei et al. about the formation of oxide phases after calcination at 450 °C of the materials of different Cu/(Cu + Mn) ratio [28]. However, characteristic peaks due to the Cu-Mn spinel phase were not

registered in the XRD patterns, probably because of the undetectable small crystallite size and/or small amount.

A significant decrease in intensity of the main CuO diffractions was observed after modification with gold. Reflections due to the presence of crystalline gold particles were not discernible. It is known that the location of the most intense peak of Au associated with the (111) plane is at $2\theta = 38.2^\circ$. In this case, an intense CuO (111) reflection lying at the same angle would preclude the exact gold identification even if any peak existed. However, the lack of reflections at $2\theta = 44.4$ and 62.6° allows one to assume a high dispersion of the gold particles.

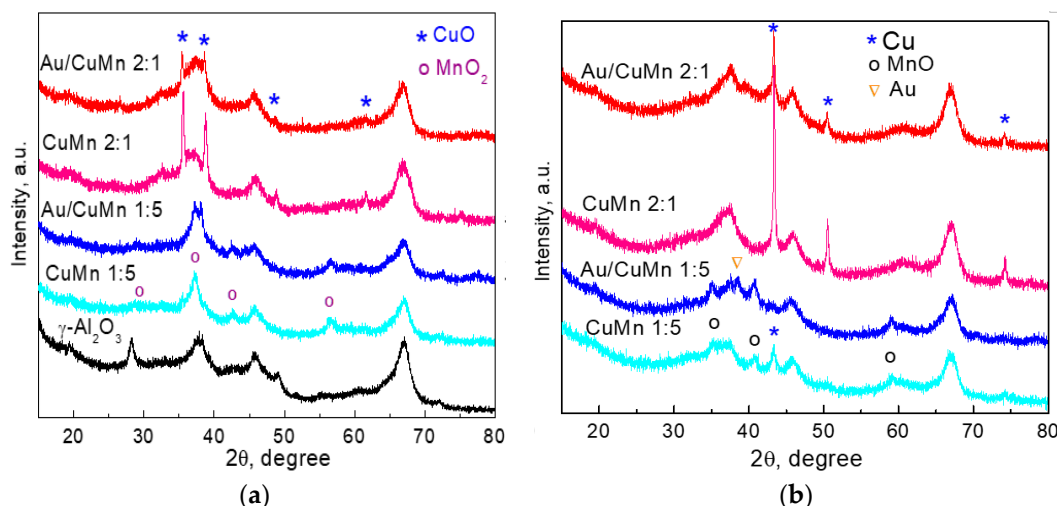


Figure 2. The powder X-ray diffraction (XRD) patterns of fresh (a) and WGS-tested (b) samples.

Analysis of the XRD patterns of the samples tested in the WGS reaction (Figure 2b) revealed significant phase changes. Sharp reflections at $2\theta = 43.3$, 50.4 , and 74.1° indicated that during the reaction the separate phase of CuO in the Cu-rich samples was reduced to Cu^0 , while MnO_2 in the samples with a Cu-to-Mn ratio of 1:5 was reduced to MnO (peaks at $2\theta = 34.9$, 40.6 , and 58.7°). It was observed that the presence of gold affected the crystallite size of metallic copper. Calculations showed about 31 nm in Au/CuMn (2:1) while, in the CuMn (2:1) sample, it was two-fold higher (62 nm). The formation of copper particles of a higher dispersion on the most active sample agrees well with the observation of Tanaka et al. [3] for the relationship between highly dispersed Cu species formed after the reduction of Cu–Mn spinel oxides and high CO conversion during the WGS reaction. A further observation that contributed to explaining the catalytic behavior of the studied catalysts was the appearance of a weak reflection at $2\theta = 38.4^\circ$ in the diffractogram of Au/CuMn (1:5). This peak corresponds to metallic gold particles of a 7 nm average size, while no such a peak was detected for the Au/CuMn (2:1) catalyst, thus confirming the stability of the highly dispersed gold particles during the reaction. A careful inspection was focused on the diffractogram of this sample, in particular on the peak at 39.4° , in order to clarify a possible formation of Au–Cu alloy. The analysis showed that this peak is due to the alumina support. Concerning the peak broadening at $2\theta = 36^\circ$ in the pattern of CuMn (2:1) in comparison with that of the Au/CuMn (2:1) sample, it could be related to the presence of Cu_2O by implying that gold facilitated CuO reduction to Cu^0 .

As it was already mentioned, both the Au and Cu crystallite particle size and resistance to aggregation during operation play a key role in the catalytic performance. In this context, the XRD data provided relevant information about the better WGS performance of the gold-promoted CuMn (2:1) sample.

2.2.4. High-Resolution Transmission Electron Microscopy (HRTEM)

HRTEM measurements and Selected area electron diffraction (SAED) patterns experimentally confirmed the presence of the nonstoichiometric $\text{Cu}_{1.5}\text{Mn}_{1.5}\text{O}_4$ spinel phase in both alumina-supported Cu-Mn mixed oxides. In the HRTEM images of Au/CuMn (2:1), well-defined lattice fringes were observed and the measured interplanar distances of 1.90 Å, 1.69 Å, and 2.07 Å closely correspond to the (331), (422), and (400) lattice planes of cubic $\text{Cu}_{1.5}\text{Mn}_{1.5}\text{O}_4$ (Figure 3a). The presence of a separate CuO phase was also recognized after measuring the distances among the lattice fringes in an HRTEM image of this sample in a different region (Figure 3b). Elemental mapping analysis clearly showed a homogeneous distribution of all elements investigated (Cu, Mn, Al, O, and Au) in Au/CuMn (2:1) (Figure S3).

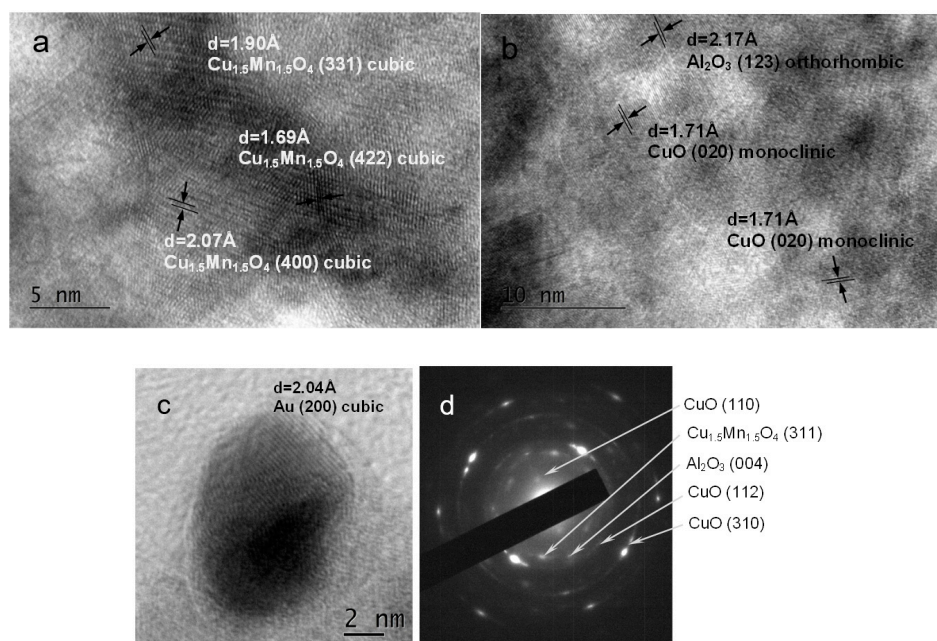


Figure 3. The High-resolution transmission electron microscopy (HRTEM) micrograph of a fresh Au/CuMn (2:1) catalyst at a magnification of 600 k (a,b) and the corresponding Selected area electron diffraction (SAED) patterns (d). The presence of the gold particle is also shown in (c) (magnification 800,000×).

The coexistence of metallic Cu and CuO particles on an Au/CuMn (2:1) sample during WGS reaction is demonstrated in Figure 4. This observation will be further discussed in relation to the data obtained by means of EPR and TPR. It could be suggested that $\text{Cu}_{1.5}\text{Mn}_{1.5}\text{O}_4$ was decomposed because its crystalline phases were not identified by TEM.

TEM images and matching SAED patterns of fresh Au/CuMn (1:5) catalyst are shown in Figure 5. As it was noted above, phase identification of the SAED patterns revealed the presence of $\text{Cu}_{1.5}\text{Mn}_{1.5}\text{O}_4$ spinel together with the MnO_2 phase in good agreement with thermal analysis. A homogeneous distribution of all elements investigated (Cu, Mn, Al, O, and Au) was also shown by elemental mapping analysis of Au/CuMn (1:5) (Figure S4).

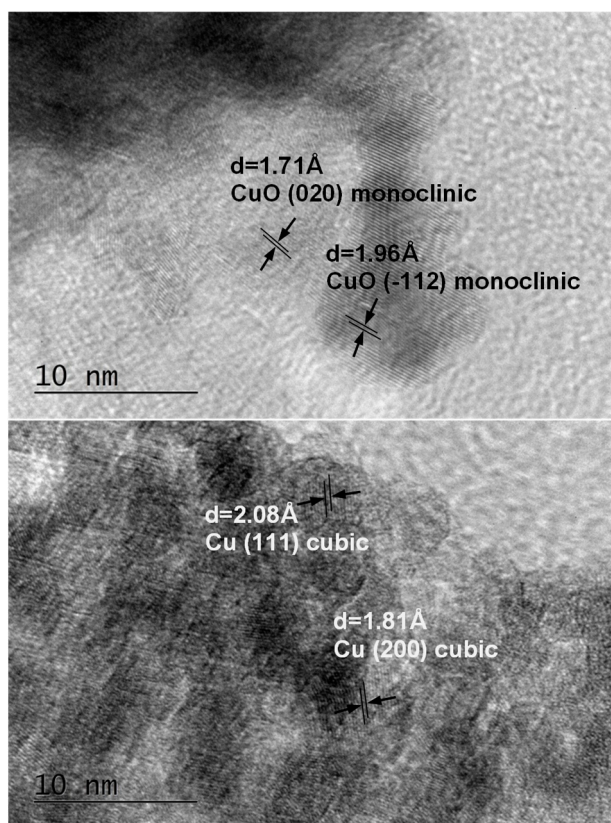


Figure 4. The HRTEM micrographs of Au/CuMn (2:1) catalyst tested in a WGS reaction at a magnification 600,000 \times .

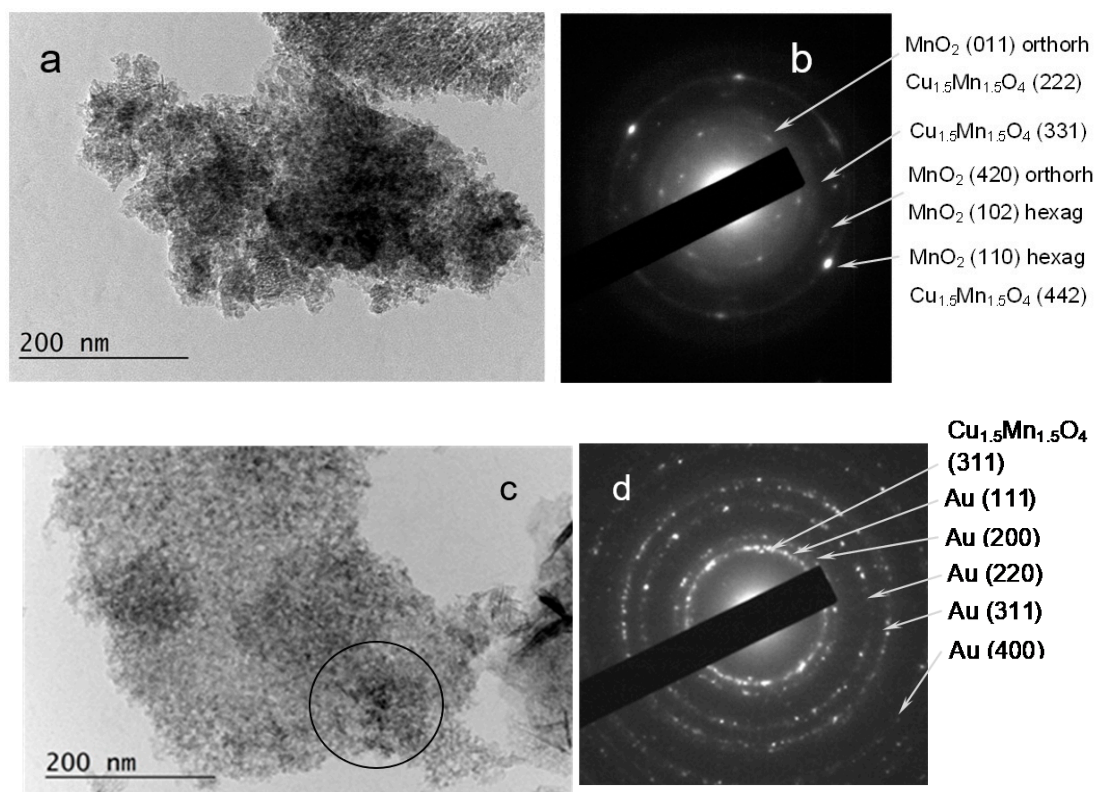


Figure 5. The TEM micrographs of fresh Au/CuMn (1:5) catalyst at a magnification of 40,000 \times (a,c) and the related SAED patterns indicating the presence of $\text{Cu}_{1.5}\text{Mn}_{1.5}\text{O}_4$ (b) and Au (d).

An HRTEM image and a corresponding SAED pattern of Au/CuMn (1:5) sample after testing in WGS reaction are displayed in Figure 6. Analysis of SAED indicated the existence of cubic MnO and Mn₃O₄. However, in contrast to the observations of Au/CuMn (2:1), lattice fringes of cubic Cu_{1.5}Mn_{1.5}O₄ were found in the HRTEM image of this sample. This finding coincides with the previously reported HRTEM analysis of a Cu-Mn spinel oxide sample after WGS reaction, where higher phase heterogeneity was one of the reasons for a lower catalytic activity [9].

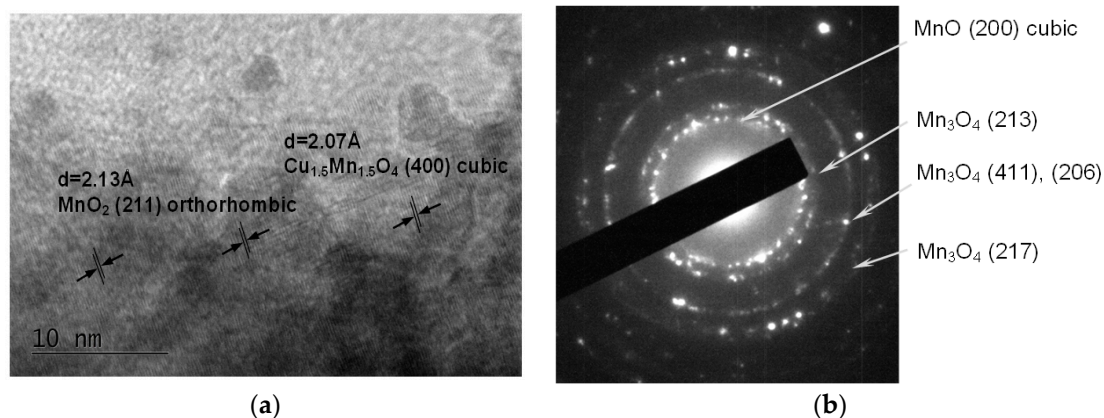


Figure 6. The HRTEM image at a magnification of 600,000 \times (a) and the SAED pattern (b) of the Au/CuMn (1:5) catalyst tested in the WGS reaction.

2.2.5. Electron Paramagnetic Resonance (EPR)

EPR spectroscopy was used to acquire more details about the nature of the active phase species. EPR spectra of fresh alumina-supported Cu–Mn mixed oxides of Cu:Mn ratio of 2:1 and 1:5 and respective Au/CuMn catalysts, as well as of their counterparts after WGS reaction, are presented in Figure 7. A typical EPR signal due to Cu²⁺ ions was observed in the spectra of all fresh catalysts (spectra a). Usually, a hyperfine structure due to the coupling between the electron spin and the nuclear spin of the Cu²⁺ ions ($S = 1/2$, $I = 3/2$) with four parallel and four perpendicular hyperfine components would be expected in the EPR spectrum of Cu²⁺ ions. In this case, the spectra of fresh samples showed a poorly resolved hyperfine structure in the parallel band at $g_{\parallel} = 2.3572$ and an unresolved one in the perpendicular band located at $g_{\perp} = 2.1029$. The values of g_{\parallel} and g_{\perp} satisfied the relation $g_{\parallel} > g_{\perp} > g_e = 2.0023$ (g_e represents the g value of a free electron) indicating that the Cu²⁺ ions are coordinated by six ligand atoms in an axially distorted octahedron [29]. The appearance of the hyperfine structure was due to isolated Cu²⁺ ions whereas the lack of hyperfine components in the perpendicular region indicated a dipolar interaction between the copper ions to form small metal oxide clusters [30]. Therefore, the isolated Cu²⁺ ions and aggregates of Cu²⁺ ions were observed in the EPR spectra of fresh catalysts. Analysis of the EPR spectra indicated that the local environment of neighboring Cu²⁺ ions is affected by the copper quantity. The EPR signal intensity decreased and the hyperfine resolution was less noticeable in the spectrum of CuMn (1:5). At the same time, the lacking characteristic signal of the manganese ions revealed that their oxidation state was Mn(IV). The deposited Au affected the intensity of the spectrum of a copper-rich sample, however, keeping the shape of the EPR lines. Spectra intensity is a measure of the quantity of paramagnetic ions and therefore it indicates variation for the Cu²⁺ ion amount. In view of decreased signal intensity in the spectrum of Au/CuMn (2:1), it could be concluded that the gold modifier contributed to the formation of EPR silent Cu⁺ sites.

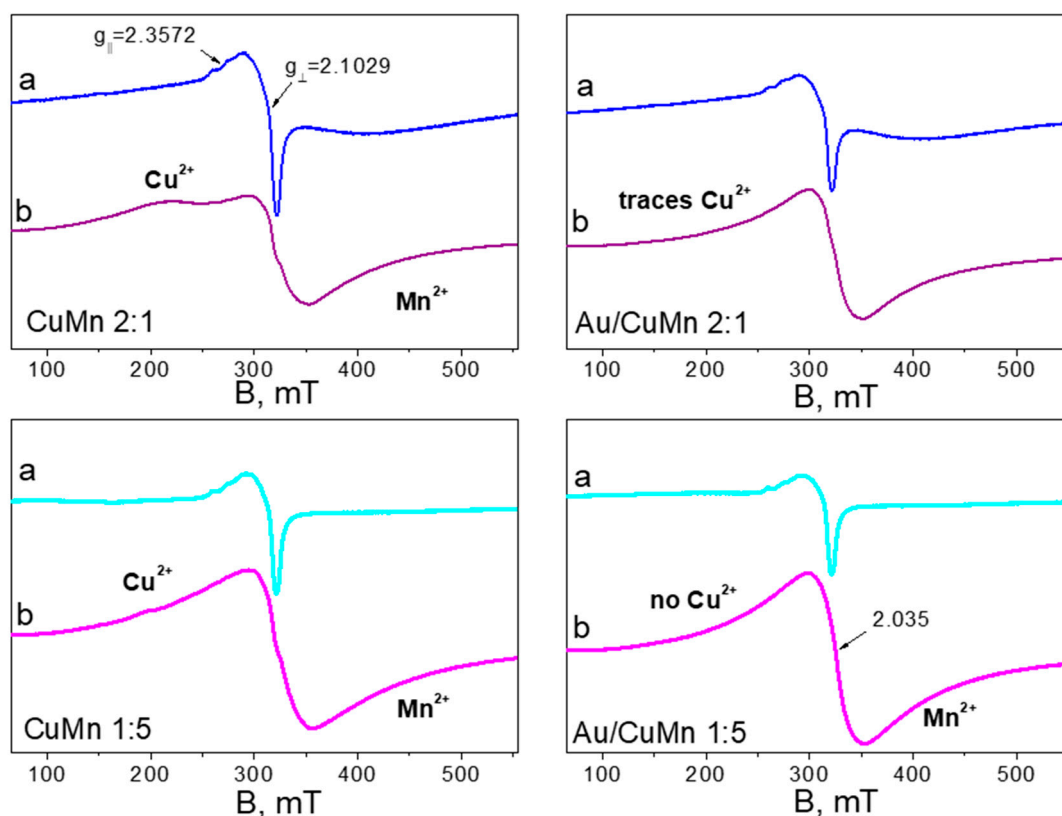


Figure 7. The Electron paramagnetic resonance (EPR) spectra of alumina-supported CuMn and Au/CuMn catalysts with a Cu:Mn ratio of 2:1 and 1:5: (a) fresh samples; (b) samples after WGS reaction.

The EPR spectra of the catalysts after WGS reaction evidenced the occurrence of some changes during the catalytic measurements (spectra b). The main feature of the spectra was an asymmetrical line with resonance absorption at $g \sim 2$. The spectra of both CuMn (2:1 and 1:5) and Au/CuMn (2:1) were a superposition of two lines of similar parameters. One of them resulted from traces of Cu^{2+} ions, while the other one located at $g = 2.035$ was associated with the presence of Mn^{2+} ions. The line of the copper ions was better visible in the spectrum of CuMn (2:1) than that of a CuMn (1:5) sample, and hardly noticeable in the spectrum of Au/CuMn (2:1). Paramagnetic Cu^{2+} ions were not observed in the spectrum of Au/CuMn (1:5). These results implied the role of gold to favor copper(II) reduction to diamagnetic copper(I) ions and are in good agreement with XRD and HRTEM analyses. The spectrum of gold-promoted manganese-rich Au/CuMn (1:5) sample represented a singlet line with a g value of 2.035 due to the availability of Mn^{2+} ions. The higher intensity of this signal in the spectra of both samples with a Cu:Mn ratio of 1:5 corresponded to a higher manganese content in these catalysts.

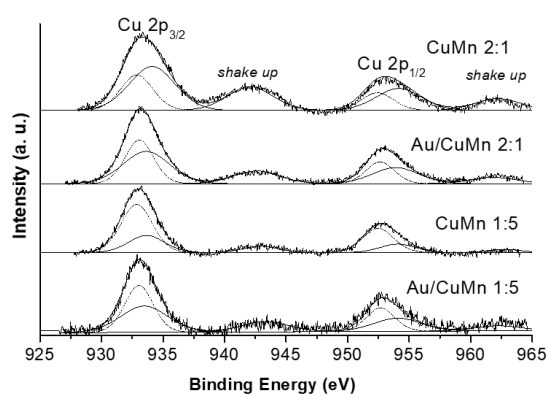
2.2.6. X-Ray Photoelectron Spectroscopy (XPS)

The oxidation state of the chemical species at the surface of the alumina-supported Cu-Mn oxides of different compositions, as well as of the gold-containing samples, was studied by means of X-ray photoelectron spectroscopy. The main results evaluated from the spectral analysis are listed in Table 3. The support Al 2p binding energy, set at 74.8 eV, was taken as internal reference for charge correction. The curve fitting analysis showed the simultaneous presence of the Cu(I), Cu(II), Mn(III), and Mn(IV) species in all samples, thus confirming once again a spinel phase formation.

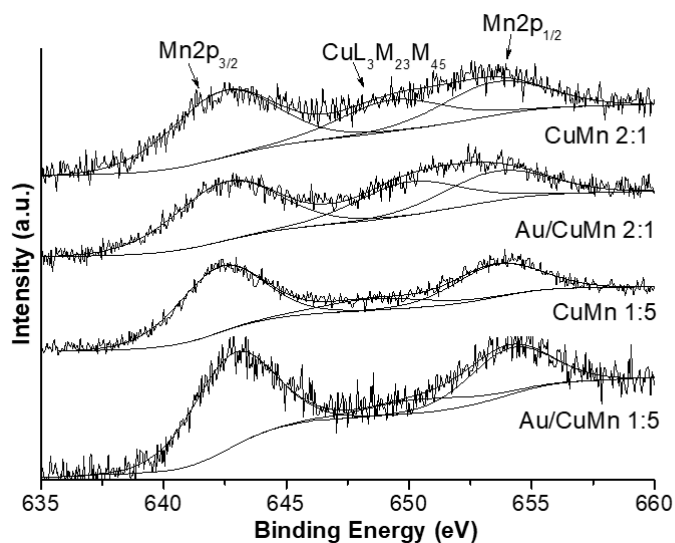
Table 3. X-ray photoelectron spectroscopy (XPS) data of the samples.

Sample	BE Cu 2p _{3/2} (eV)	BE Mn 2p _{3/2} (eV)	BE Au 4f _{7/2} (eV)	Cu/Mn	Cu/Al	Au/Cu	Au/ (Cu + Mn)	Sat/Cu 2p
Cu-Mn 2:1	932.7 933.9	642.4	-	2.4	0.07	-	-	0.27
Cu-Mn 1:5	932.9 933.6	642.2	-	1.4	0.03	-	-	0.18
Au/Cu-Mn 2:1	932.7 933.7	642.5	84.8	2.1	0.04	0.06	0.04	0.14
Au/Cu-Mn 1:5	932.9 933.6	642.3	84.7	1.1	0.02	0.29	0.10	0.13

Figure 8 presents the background-subtracted fitted Cu 2p_{3/2} spectra of all samples. The fitting procedure allowed obtaining two Cu 2p components: a low energy component at about 932.7 eV attributable to Cu(I), and a high energy component at 933.8 eV which, along with the shake-up peaks, is characteristic of Cu(II) [31].

**Figure 8.** The Cu 2p XP spectra of alumina-supported CuMn mixed oxides and gold-containing catalysts.

Mn 2p_{3/2} spectra are shown in Figure 9. Because of the variety of possible oxidation states, the interpretation of the manganese oxidation state is rather complicated. A typical position of the Mn(IV) binding energy of 642.5 ± 0.1 eV was obtained. However, a contribution from Mn(III) could be assumed on the basis of a rather broad linewidth of the peak (4.4 eV).

**Figure 9.** The Mn 2p XP spectra of alumina-supported CuMn mixed oxides and gold-containing catalysts.

The Au 4f_{7/2} peak centered at 84.7 ± 0.1 eV in the XP spectra of both samples indicated the presence of a positively charged gold species. Figure S5 shows the Au 4f spectra of both gold catalysts. Concerning the XPS-derived atomic ratios, it is worth noticing that the surface was enriched in copper with respect to manganese. Indeed, particularly for the CuMn (1:5) sample, the Cu-to-Mn atomic ratio is much higher than the analytical value of 0.2. Moreover, the slight but consistent decrease of the ratio observed with the gold catalysts suggests a preferential localization of the gold over the copper sites. As suggested from the Au/(Cu + Mn) data and also from Au/Al (the latter not listed in the table), a higher surface concentration of the gold species is observed for the Au/CuMn (1:5) sample. Furthermore, in accordance with the EPR results and the XPS data shown in Figure 8 and Table 3 (Sat/Cu2p column), the relative Cu(I)/Cu(II) concentration increases in the presence of gold. Certainly, the Sat/Cu2p ratio, being an intensity relation of the typical Cu(II) shake-up feature to the main Cu 2p peak, decreases upon the deposition of gold.

2.2.7. Temperature-Programmed Reduction (TPR)

H₂-TPR profiles of fresh (a) and WGS-tested (b) alumina-supported copper-manganese mixed oxides with a Cu-to-Mn ratio of 2:1 and 1:5 and gold-promoted samples are shown in Figure 10. It has been reported that the reduction of bulk CuO proceeds in a single step process with T_{max} at about 300 °C [31]. A complex peak with two components (T_{max} at 193 and 259 °C) characterized the reduction profile of Cu/Mn (2:1). The lower temperature component was assigned to the reduction of a separate CuO phase that was registered by XRD. A significant shift of T_{max} to a lower temperature in comparison with that of bulk CuO clearly indicated the presence of highly dispersed CuO particles. The second broad component with two maxima at 243 °C and 259 °C was associated with the reduction of both larger CuO particles and the Cu-Mn spinel phase. This assignment is in harmony with the analysis of the EPR spectra about the co-existence of two different types of Cu²⁺ sites due to the formation of isolated Cu(II) ions and agglomerated CuO. The higher temperature component (259 °C) should be related to the reduction of a highly dispersed Cu-Mn spinel phase of relatively small crystallite size [32]. Our TPR results are consistent with the observations of Li et al. [33] who have studied CuMn_(y)O_x/γ-Al₂O₃ of the same amount of active phase as in the present work (20 wt %) and have registered one TPR reduction peak up to 300 °C. Tanaka et al. have also reported the reduction of Cu_{1.5}Mn_{1.5}O₄ in the temperature range of 300–500 °C depending on the preparation method [4].

The reduction profile of CuMn with a ratio of 1:5 exhibited a peak with well-defined T_{max} at 290 °C that was attributed to the reduction of Cu_{1.5}Mn_{1.5}O₄ [11]. A significantly enhanced reducibility was ascribed to the promotional role of copper on the reduction of Mn ions in the spinel [3,31]. According to Morales et al., structural defects associated with oxygen vacancies, as well as the high dispersion of separate MnO_x phase, have an additional effect on the facilitated reduction of MnCu_x catalysts [34]. A broad shoulder on the low-temperature side of the profile could be related to the reduction of copper oxide species.

The modification with gold affected the reducibility of both Cu-Mn mixed oxides irrespective of their composition. A strong reduction peak was registered in the profile of Au/CuMn (2:1), which was assigned to the simultaneous reduction of copper oxide and the spinel phase. Considering the composition of the second sample, i.e., Au/CuMn (1:5), a profile of a similar shape as that of the sample without gold was observed, however, significantly shifted to a lower temperature. It was ascribed to the reduction of MnO₂ and spinel phase. It should be noted that in both gold-based samples the reduction of the spinel phase was completed at a lower temperature in comparison with that of the alumina-supported Cu-Mn oxides. The promotional role of gold on the reducibility of the spinel phase could be explained with the ability of the nanosized gold particles to activate hydrogen and consequently atomic hydrogen spillover onto the support [35]. Additionally, by means of FTIR spectroscopy, it was demonstrated that hydrogen dissociation might occur on gold sites even at room temperature and the active hydrogen atoms might reduce the support surface sites in the close

vicinity [36]. However, the enhanced reducibility of the spinel phase in the presence of gold could also be related to the improved mobility of the oxygen with successive formation of oxygen vacancies.

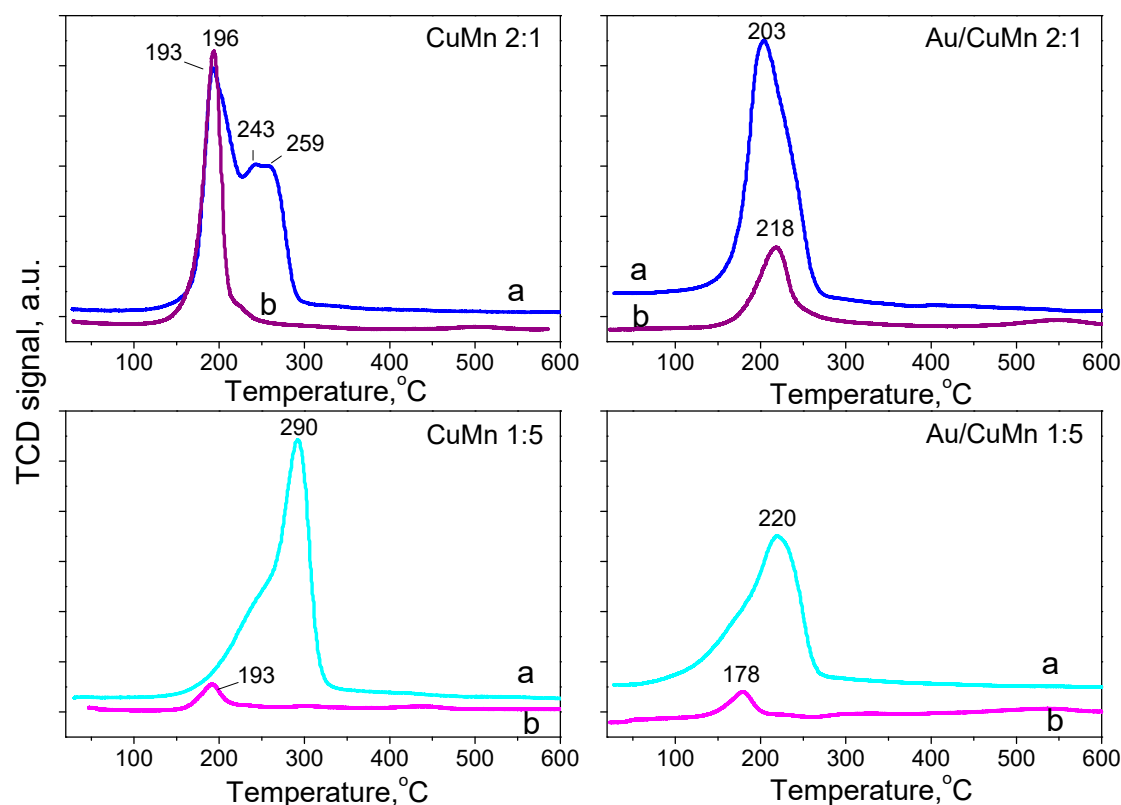


Figure 10. TPR profiles of alumina-supported CuMn and Au/CuMn catalysts with a Cu-to-Mn ratio of 2:1 and 1:5: (a) fresh samples; (b) samples after the WGS reaction.

TPR profile analysis of all samples after WGS testing is consistent with XRD, HRTEM, and EPR data (Figure 10, profiles b). The narrow peak in the profile of the copper-rich sample overlapped very well the first component in the profile of the fresh sample. At the same time, the disappearance of the second broad component allowed to assume complete decomposition of the spinel phase under WGS conditions. A separate CuO phase was not observed by XRD and only the presence of Cu₂O was suggested. However, in the EPR spectrum of CuMn (2:1), a well visible signal related to copper(II) ions was registered. The reduction process could be associated with the reduction of both CuO and Cu₂O. Despite the homogeneous distribution of all elements (EDS mapping), this finding revealed that the composition of this sample is not favorable for the formation of highly dispersed copper particles. The promotion by gold facilitated the reduction as evidenced by the low-intensity TPR peak in the profile of the WGS-tested Au/CuMn (2:1) catalyst. This interpretation is in agreement with the EPR-observed traces of Cu²⁺ and higher dispersion of metallic copper particles calculated based on XRD reflections. The TPR profiles of both the manganese-rich samples used in the WGS reaction consisted of one very weak peak of a similar shape. In this case, the hydrogen consumption should be related to the reduction of both some CuO particles as indicated by EPR for CuMn (1:5) and small amounts of Mn₃O₄ (HRTEM). Both EPR and HRTEM (SAED) techniques evidenced a nearly complete transformation of the spinel phase to MnO. According to the literature, the further reduction of MnO to Mn⁰ has not occurred even up to 950 °C [32].

Following the goal of the present study, i.e., to develop a catalytically efficient and economically viable formulation, we could suggest a promising catalytic material for low-temperature WGS reaction based on gold-promoted Cu-Mn mixed oxides supported on alumina. It was demonstrated that the Cu:Mn molar ratio at the surface of the alumina affected the WGS behavior only after the addition of

gold, thus implying the key role of highly dispersed gold nanoparticles. In a very recent work, we have studied the state of the surface species in real reaction conditions by FTIR spectroscopy [37]. Spectra were collected after the admission of carbon monoxide at about $-180\text{ }^{\circ}\text{C}$ over alumina-supported CuMn (2:1) and Au/CuMn (2:1). Comparison revealed that gold strongly affected the nature of the exposed sites and their adsorption ability owing to an extremely enhanced reactivity towards CO oxidation. By applying several techniques to characterize the samples before and after WGS tests, it could be concluded that the favorable effect of gold is related not only to the activation of CO, but also to the enhancement of CuO reducibility. Ratnasamy and Wagner have summarized recent developments in WGS catalysis and assumed that small copper clusters are the active sites for the WGS reaction [1]. Therefore, the growth of the small crystallites into larger entities would be the reason for the depletion of the active sites. According to Tanaka et al., the stabilization of small metallic copper particles by the host manganese oxides is of particular importance for high WGS activity [3]. The best performance of a gold-promoted sample with a Cu-to-Mn ratio of 2:1 might be related to the beneficial role of Au on spinel decomposition and formation of highly dispersed copper particles during the reaction, thus ensuring the presence of two highly dispersed active metallic phases. Upon analyzing both the gold and copper particle sizes, a question arises about the role of the alumina-supported mixed oxides to prevent gold particle agglomeration during the WGS operation conditions. XRD analysis of the WGS-examined samples indicated that the composition of CuMn (2:1) is more appropriate for keeping a higher gold dispersion. Cooperative effects in the adsorption and activation of CO and water should also be taken into consideration. According to some experimental and theoretical works, water dissociation plays an important role in the WGS reaction. In this sense, an alumina-supported Cu-Mn mixed oxide with good redox properties contributed to water dissociation. Thus, the improved catalytic activity was achieved through the synergistic action of both gold and copper particles as well as metal-support interaction. Future efforts could be focused on the optimization of the amount of supported active phase and gold loading.

3. Materials and Methods

3.1. Sample Preparation

Alumina-supported copper oxide, manganese oxide, and Cu-Mn mixed oxides with Cu-to-Mn molar ratios of 1:5 and 2:1 were prepared by wet impregnation. Prior to the impregnation, the γ -alumina support (0.6–1.0 mm grain size) was thermally treated at $450\text{ }^{\circ}\text{C}$ for 2 h. The content of transition metal oxides phase was 20 wt.%. Impregnation was carried out at room temperature by the addition of an aqueous solution of copper or manganese nitrate, or a mixture of the nitrates of preset ratio to $\gamma\text{-Al}_2\text{O}_3$. The suspensions were kept at $80\text{ }^{\circ}\text{C}$ for 12 h. The preparation procedure included drying at RT for 12 h, heating at $120\text{ }^{\circ}\text{C}$ for 10 h, calcination at $450\text{ }^{\circ}\text{C}$ for 4 h by a temperature rise from $120\text{ }^{\circ}\text{C}$ at a rate of $10\text{ }^{\circ}\text{C min}^{-1}$. Both alumina-supported Cu-Mn mixed oxides were denoted as CuMn (2:1) and CuMn (1:5) depending on the Cu-to-Mn molar ratio.

Modification by gold was carried out by deposition-precipitation of 2 wt % Au on alumina-supported Cu-Mn mixed oxides. A 0.06-M solution of $\text{HAuCl}_4 \cdot 3\text{H}_2\text{O}$ and a 0.2-M solution of Na_2CO_3 were left to interact at a constant pH of 7, temperature of $60\text{ }^{\circ}\text{C}$, stirring speed of 250 rpm, and reactant feed flow rate of 0.15 L h^{-1} . The precipitates were filtered, washed, dried under vacuum at $80\text{ }^{\circ}\text{C}$, and calcined in air at $400\text{ }^{\circ}\text{C}$ for 2 h. The gold catalysts were denoted as Au/CuMn (2:1) and Au/CuMn (1:5).

3.2. Sample Characterization

The textural characteristics were determined by low temperature ($-196\text{ }^{\circ}\text{C}$) nitrogen adsorption on a Quantachrome Instrument NOVA 1200e (Quantachrome Instruments, Boynton Beach, FL, USA) specific surface area and pore analyzer. The total pore volume and pore diameter were determined at

a relative pressure close to 0.99. Specific surface areas (S_{BET}) were estimated through the Brunauer, Emmett, and Teller (BET) method in a standard pressure range $p/p_0 = 0.10\text{--}0.30$.

Thermal analysis (TG, DTG, and DTA) was performed on a Stanton Redcroft computerized thermal installation (Stanton Redcroft LTD, London, UK) under the following experimental conditions: temperature interval of 20–650 °C, heating rate of 10 °C min⁻¹, sample weight of 12.00 mg, gas environment—100% air, pot—stabilized corundum.

Phase identification was determined by means of an X-ray powder diffraction (XRD) PANalytical Empyrean apparatus (PANalytical B.V., Almelo, The Netherlands) equipped with a multichannel detector (Pixel 3D) (PANalytical B.V., Almelo, The Netherlands), using (Cu K α 45 kV–40 mA) radiation in the 20–100° 2 θ range, with a scan step of 0.01 for 20 s. The cell refinements were obtained with the PowderCell program.

Transmission electron microscopy (TEM) analysis was performed by a JEOL JEM 2100 instrument (JEOL, Tokyo, Japan) at an accelerating voltage of 200 kV. Selected area electron diffraction (SAED) and HRTEM were also employed to receive information on the nature of the crystalline phases. Phase identification of SAED patterns was accomplished by the PCPDFWIN computer program and the PDF-2 Database of International Center for Diffraction Data. The catalytic materials, fresh and used in WGS reaction, were subjected to a preliminary preparation procedure for TEM analysis. Microquantities of all samples were suspended in double distilled water in separate glass containers and ultrasonicated for 3 min. A drop of suspension for each sample was fixed on a standard copper grid covered by an amorphous carbon membrane and left to dry for 24 h in a vacuum chamber at room temperature. After that, they were introduced to the microscope chamber for TEM study.

Electron paramagnetic resonance (EPR) measurements were performed at room temperature using a JEOL JES-FA 100 EPR spectrometer (JEOL, Tokyo, Japan) operating at the X band (~9.8 GHz). The magnetic field was modulated at 100 kHz and the g values were determined from precise frequency and magnetic field values. The samples were placed in a quartz tube and were fixed in the center of a standard TE₀₁₁ cylindrical resonator. The EPR cavity had a microreactor cell specially designed for high-temperature measurements. To evaporate moisture, the spectra were firstly recorded at 120 °C and then cooled down to room temperature. The desired temperature was monitored by a JEOL DVT controller (JEOL, Tokyo, Japan). The microwave power was sufficiently small to avoid saturation effects.

X-ray photoelectron spectroscopy (XPS) analyses were performed by means of a VG Microtech ESCA 3000 Multilab (VG Scientific, Sussex, UK.) device equipped with unmonochromatized Al K α source (1486.6 eV). The sample powders, mounted on a double-sided adhesive tape, were degassed overnight inside the high vacuum preparation chamber before being analyzed. The CASA XPS software (version 2.3.17, Casa Software Ltd. Wilmslow, Cheshire, UK, 2009) was employed for the qualitative and quantitative analyses of the experimental spectra [38]. The binding energy values are quoted with a precision of ± 0.15 eV, and the atomic percentage with a precision of $\pm 10\%$.

TPR measurements were conducted in a flow system under the following conditions: hydrogen-argon gas mixture (10% H₂); temperature ramp rate of 15 °C min⁻¹; flow rate of 24 mL min⁻¹, and a sample amount of 0.05 g.

3.3. Catalytic Activity Measurements

WGS activity measurements were carried out in a flow reactor at atmospheric pressure over a temperature range of 120–260 °C. The reactant gas mixture fed into the reactor contained 3.37 vol % CO, 25.01 vol % H₂O, and 71.62 vol % Ar. The concentration of water vapor in the gas mixture was controlled by a Syringe pump RAZEL model R-99 (Razel Scientific Instruments, a part of Mansfield Research and Development, Saint Albans, VT, USA) with a 10-cm³ syringe for very accurate flow. The following conditions were applied: a catalyst bed volume of 0.5 cm³ (0.6–1.0 mm grain size) and a space velocity of 4000 h⁻¹. An Uras 3G (Hartmann&Braun AG, Frankfurt am Main, Germany)

gas analyzer measured the CO content at the reactor outlet. The CO conversion was calculated based on inlet and outlet CO concentration.

4. Conclusions

A successful design of cost-effective and catalytically efficient WGS catalysts was achieved by the combination of γ -alumina modified with a surface fraction of Cu–Mn mixed oxides and gold nanoparticles. The comparison of WGS activity of the supported mono (CuO or MnO₂) and mixed metal oxides clearly showed a synergistic effect over the Cu–Mn mixed oxides. The composition of the supported mixed oxides contributed to water dissociation due to their good redox properties and influenced the formation of highly dispersed gold and copper particles under reaction conditions in a different way. The beneficial role of nanosized gold was related not only to the appearance of new active sites for CO activation, but also to the enhancement of CuO reducibility and nonstoichiometric spinel phase decomposition. The promotional effect of gold was better demonstrated in the case of the Cu-rich sample, i.e., with a Cu-to-Mn molar ratio of 2:1. A higher activity resulted from the presence of two finely dispersed active metallic phases. The composition of the Cu-rich sample ensured the abundance of highly dispersed copper particles and stabilization of nanosized gold particles on high-surface-area alumina-supported Cu–Mn mixed oxides. In contrast, gold particles of an average size of about 7 nm were formed on the surface of manganese-rich samples. The WGS activity in the low-temperature range and the stability over a period of 32 h, as well as after exposure to air, opens the possibility for the potential application in fuel cell technology.

Supplementary Materials: The following are available online at <http://www.mdpi.com/2073-4344/8/11/563/s1>, Figure S1. Stability test of Au/CuMn (2:1) catalyst performed for 32 h at 260 °C; Figure S2. Thermal analysis of: (a) CuMn (2:1), (b) CuMn (1:5); Figure S3. Representative STEM image and relative XEDX mapping distribution of all components over Au/CuMn (2:1) catalyst. Figure S4. Representative STEM image and relative XEDX mapping distribution of all components over Au/CuMn (1:5) catalyst. Figure S5. Au 4f XP spectra of gold catalysts on alumina-supported Cu–Mn mixed oxides.

Author Contributions: T.T.: results analysis, manuscript preparation, and funding acquisition; I.I.: catalytic experiments; Y.K.: performed and discussed EPR analysis; D.K.: HRTEM measurements and analysis, A.M.V. performed and discussed XPS analysis; P.P. H₂-TPR measurements; G.A. performed XRD analysis; E.K. and K.I.: materials synthesis and thermal analysis. All authors contributed to discussion of the manuscript.

Funding: This research and APC was funded by Bulgarian National Science Fund grant number $\overline{A}H$ 09/5/2016.

Conflicts of Interest: The authors declare no conflict of interest. The funders had no role in the design of the study; in the collection, analyses, or interpretation of data; in the writing of the manuscript, and in the decision to publish the results.

References

1. Ratnasamy, C.; Wagner, J.P. Water gas shift catalysis. *Catal. Rev. Sci. Eng.* **2009**, *51*, 325–440. [[CrossRef](#)]
2. Pal, D.B.; Chand, R.; Upadhyay, S.N.; Mishra, P.K. Performance of water gas shift reaction catalysts: A review. *Renew. Sustain. Energy Rev.* **2018**, *93*, 549–565. [[CrossRef](#)]
3. Tanaka, Y.; Utaka, T.; Kikuchi, R.; Takeguchi, T.; Sasaki, K.; Eguchi, K. Water gas shift reaction for the reformed fuels over Cu/MnO catalysts prepared via spinel-type oxide. *J. Catal.* **2003**, *215*, 271–278. [[CrossRef](#)]
4. Tanaka, Y.; Takeguchi, T.; Kikuchi, R.; Eguchi, K. Influence of preparation method and additive for Cu–Mn spinel oxide catalyst on water gas shift reaction of reformed fuels. *Appl. Catal. A* **2005**, *279*, 59–66. [[CrossRef](#)]
5. Zhi, K.; Liu, Q.; Zhang, Y.; He, S.; He, R. Effect of precipitator on the texture and activity of copper-manganese mixed oxide catalysts for the water gas shift reaction. *J. Fuel Chem. Technol.* **2010**, *38*, 445–451. [[CrossRef](#)]
6. He, R.-X.; Liu, Q.-S.; Zhi, K.-D.; Cui, X.-L. Effect of adding rate of precipitator on the texture and activity of the copper-manganese mixed oxide catalyst for water gas shift reaction. *J. Fuel Chem. Technol.* **2008**, *36*, 767–771.
7. He, R.-X.; Zhi, K.-D.; Wang, B.; Wu, F.; Jiang, H.-Q.; Liu, Q.-S. Influence of copper-manganese salt precursors on catalytic performance of copper-manganese catalysts for water-gas shift reaction. *J. Mol. Catal.* **2015**, *29*, 534–544.

8. Zhi, K.; Liu, Q.; He, R.; Wu, F.; Zhang, Y.; Yang, L. Effect of the ration of Cu to Mn on the activity and stability of copper-manganese mixed-oxides for the water gas shift reaction. *Adv. Mater. Res.* **2013**, *634–638*, 518–521. [[CrossRef](#)]
9. Tabakova, T.; Idakiev, V.G.; Avgouropoulos, G.; Papavasiliou, J.; Manzoli, M.; Boccuzzi, F.; Ioannides, T. Highly active copper catalyst for low-temperature water-gas shift reaction prepared via a Cu-Mn spinel oxide precursor. *Appl. Catal. A* **2013**, *413*, 184–191. [[CrossRef](#)]
10. Du, X.; Yuan, Z.; Cao, L.; Zhang, C.; Wang, S. Water gas shift reaction over Cu-Mn mixed oxides catalysts: Effects of the third metal. *Fuel Proc. Technol.* **2008**, *89*, 131–138. [[CrossRef](#)]
11. He, R.; Wang, D.; Zhi, K.; Wang, B.; Zhong, H.; Jiang, H.; Li, N.; Liu, Q. Cu-Mn catalysts modified by rare earth lanthanum for low temperature water-gas shift reaction. *J. Rare Earths* **2016**, *34*, 994–1003. [[CrossRef](#)]
12. Li, C.; Li, Z.; Oh, H.Y.; Hong, G.H.; Park, J.S.; Kim, J.M. Ordered mesoporous Cu-Mn-Ce ternary metal oxide catalysts for low temperature water-gas shift reaction. *Catal. Today* **2018**, *307*, 237–242. [[CrossRef](#)]
13. Andreeva, D.; Idakiev, V.; Tabakova, T.; Andreev, A. Low-Temperature water-gas shift reaction over Au/ α -Fe₂O₃. *J. Catal.* **1996**, *158*, 354–355. [[CrossRef](#)]
14. Fu, Q.; Weber, A.; Flytzani-Stephanopoulos, M. Nanostructured Au-CeO₂ catalysts for low-temperature water-gas shift. *Catal. Lett.* **2001**, *77*, 87–95. [[CrossRef](#)]
15. Sandoval, A.; Gomez-Cortes, A.; Zanella, R.; Diaz, G.; Saniger, J.M. Gold nanoparticles: Support effects for the WGS reaction. *J. Mol. Catal. A* **2007**, *278*, 200–208. [[CrossRef](#)]
16. Odabasi, C.; Günay, M.E.; Yildirim, R. Knowledge extraction for water gas shift reaction over noble metal catalysts from publications in the literature between 2002 and 2012. *Int. J. Hydrogen Energy* **2014**, *39*, 5733–5746. [[CrossRef](#)]
17. Tao, F.; Ma, Z. Water-gas shift on gold catalysts: Catalyst systems and fundamental studies. *Phys. Chem. Chem. Phys.* **2013**, *15*, 15260–15270. [[CrossRef](#)] [[PubMed](#)]
18. Reina, T.R.; González Castaño, M.; Palma, S.; Ivanova, S.; Odriozola, J.A. Twenty Years of golden future in the water gas shift reaction. In *Heterogeneous Gold Catalysts and Catalysis*; Ma, Z., Dai, S., Eds.; RSC Catal. Series; Royal Society of Chemistry: Cambridge, UK, 2014; Volume 18, pp. 111–140; ISBN 978-1-84973-917-7.
19. Andreeva, D.; Tabakova, T.; Ilieva, L. Ceria-based gold catalysts: Synthesis, properties and catalytic performance for the WGS and PROX processes. In *Catalysis by Ceria and Related Materials*, 2nd ed.; Trovarelli, A., Fornasiero, P., Eds.; Imperial College Press: London, UK, 2013; Volume 12, pp. 497–564; ISBN 978-1-84816-963-0.
20. Reina, T.R.; Ivanova, S.; Idakiev, V.; Delgado, J.J.; Ivanov, I.; Tabakova, T.; Centeno, M.A.; Odriozola, J.A. Impact of Ce-Fe synergism on the catalytic behaviour of Au/CeO₂-FeO_x/Al₂O₃ for pure H₂ production. *Catal. Sci. Technol.* **2013**, *3*, 779–787. [[CrossRef](#)]
21. Reina, T.R.; Ivanova, S.; Delgado, J.J.; Ivanov, I.; Idakiev, V.; Tabakova, T. Viability of Au/CeO₂-ZnO/Al₂O₃ catalysts for pure hydrogen production by the WGS. *ChemCatChem* **2014**, *5*, 1401–1409.
22. Reina, T.R.; Ivanova, S.; Laguna, O.H.; Centeno, M.A.; Odriozola, J.A. WGS and CO-PrO_x reactions using gold promoted copper-ceria catalysts: Bulk CuO-CeO₂ vs. CuO-CeO₂/Al₂O₃ with low mixed oxide content. *Appl. Catal. B* **2016**, *197*, 62–72. [[CrossRef](#)]
23. Santos, J.L.; Reina, T.R.; Ivanova, S.; Centeno, M.A.; Odriozola, J.A. Gold promoted Cu/ZnO/Al₂O₃ catalysts prepared from hydrotalcite precursors: Advanced materials for the WGS reaction. *Appl. Catal. B* **2017**, *201*, 310–317. [[CrossRef](#)]
24. Ivanov, K.I.; Kolentsova, E.N.; Dimitrov, D.Y. Alumina supported copper-manganese catalysts for combustion of exhaust gases: Effect of preparation method. *Int. J. Chem., Nucl. Mater. Metall. Eng.* **2015**, *4*, 548–557.
25. Roshan, A.C.; Irankhah, A.; Mahmoudizadeh, M.; Arandiyani, H. Single-stage water gas shift reaction over structural modified Cu-Ce catalysts at medium temperatures: Synthesis and catalyst performance. *Chem. Eng. Res. Des.* **2018**, *132*, 843–852. [[CrossRef](#)]
26. Kondrat, S.A.; Davies, T.E.; Zu, Z.; Boldrin, P.; Bartley, J.K.; Carley, A.F.; Taylor, S.H.; Rosseinsky, M.J.; Hutchings, G.J. The effect of heat treatment on phase formation of copper manganese oxide: Influence on catalytic activity for ambient temperature carbon monoxide oxidation. *J. Catal.* **2011**, *281*, 279–289. [[CrossRef](#)]
27. Pintons, D.G.; Juan, A.; Irigoyen, B. Density functional theory study of water interactions on Mn-doped CeO₂(1 1 1) surface. *Appl. Surf. Sci.* **2014**, *313*, 784–793. [[CrossRef](#)]
28. Wei, P.; Bieringer, M.; Cranswick, L.; Petric, A. In situ high-temperature X-ray and neutron diffraction of Cu-Mn oxide phases. *J. Mater. Sci.* **2010**, *45*, 1056–1064. [[CrossRef](#)]

29. Li, G.; Dimitrijevic, N.M.; Chen, L.; Rajh, T.; Gray, K.A. Role of surface/interfacial Cu²⁺ sites in the photocatalytic activity of coupled CuO-TiO₂ nanocomposites. *J. Phys. Chem. C* **2008**, *112*, 19040–19044. [[CrossRef](#)]
30. Dong, L.; Liu, L.; Lv, Y.; Zhu, J.; Wan, H.; Liu, B.; Gao, F.; Wang, X.; Dong, L.; Chen, Y. Surface structure characteristics of CuO/Ti_{0.5}Sn_{0.5}O₂ and its activity for CO oxidation. *J. Mol. Catal.* **2012**, *365*, 87–94. [[CrossRef](#)]
31. Papavasiliou, J.; Avgouropoulos, G.; Ioannides, T. Combined steam reforming of methanol over Cu–Mn spinel oxide catalysts. *J. Catal.* **2007**, *251*, 7–20. [[CrossRef](#)]
32. Dasireddy, V.D.B.C.; Valand, J.; Likozar, B. PROX reaction of CO in H₂/H₂O/CO₂ Water-Gas Shift (WGS) feedstocks over Cu-Mn/Al₂O₃ and Cu-Ni/Al₂O₃ catalysts for fuel cell applications. *Renew. Energy* **2018**, *116*, 75–87. [[CrossRef](#)]
33. Li, X.; Wang, L.; Xia, Q.; Liu, Z.; Li, Z. Catalytic oxidation of toluene over copper and manganese based catalysts: Effect of water vapor. *Catal. Commun.* **2011**, *14*, 15–19. [[CrossRef](#)]
34. Morales, M.R.; Barbero, B.P.; Cadús, L.E. Total oxidation of ethanol and propane over Mn-Cu mixed oxide catalysts. *Appl. Catal. B* **2006**, *67*, 229–236. [[CrossRef](#)]
35. Manzoli, M.; Chiorino, A.; Vindigni, F.; Boccuzzi, F. Hydrogen interaction with gold nanoparticles and clusters supported on different oxides: A FTIR study. *Catal. Today* **2012**, *181*, 62–67. [[CrossRef](#)]
36. Boccuzzi, F.; Chiorino, A.; Manzoli, M.; Andreeva, D.; Tabakova, T. FTIR Study of the Low-Temperature Water–Gas Shift Reaction on Au/Fe₂O₃ and Au/TiO₂ Catalysts. *J. Catal.* **1999**, *188*, 176–185. [[CrossRef](#)]
37. Tabakova, T.; Kolentsova, E.; Dimitrov, D.; Ivanov, K.; Manzoli, M.; Venezia, A.M.; Karakirova, Y.; Petrova, P.; Nihtianova, D.; Avdeev, G. CO and VOCs catalytic oxidation over alumina supported Cu–Mn catalysts: Effect of Au or Ag deposition. *Top. Catal.* **2017**, *60*, 110–122. [[CrossRef](#)]
38. Biesinger, M.C.; Lau, L.W.M.; Gerson, A.; Smart, R.S.C. Resolving surface chemical states in XPS analysis of first row transition metals, oxides and hydroxides: Sc, Ti, V, Cu, and Zn. *Appl. Surf. Sci.* **2010**, *257*, 887–898. [[CrossRef](#)]



© 2018 by the authors. Licensee MDPI, Basel, Switzerland. This article is an open access article distributed under the terms and conditions of the Creative Commons Attribution (CC BY) license (<http://creativecommons.org/licenses/by/4.0/>).